Tuning the Chiroptical Properties of Elongated Nano-objects via Hierarchical Organization

Jie Gao, Wenbing Wu, Vincent Lemaire, Alain Carvalho, Sylvain Nlate, Thierry Buffeteau, Reiko Oda, Yann Battie, Matthias Pauly, Emilie Pouget

Tuning the Chiroptical Properties of Elongated Nano-Objects via Hierarchical Organization

Jie Gao,[1] Wenbing Wu,[2] Vincent Lemaire,[2] Alain Carvalho,[2] Sylvain Nlate,[1] Thierry Buffeteau,[3] Reiko Oda,[1] Yann Battie,[4] Matthias Pauly*,[2] Emilie Pouget*[1]*

[1] CNRS, Univ. Bordeaux, Bordeaux INP, Chimie et Biologie des Membranes et des Nanoobjets, UMR 5248, Allée St Hilaire, Bat B14, 33607 Pessac, France

[2] Université de Strasbourg, CNRS, Institut Charles Sadron, F-67000 Strasbourg, France

[3] Institut des Sciences Moléculaires (UMR5255 ISM), CNRS - Université de Bordeaux, 351 Cours de la Libération, 33405 Talence, France

[4] LCP-A2MC, Université de Lorraine, 1 Bd Arago, 57070 Metz, France

ABSTRACT. Chiral materials appear as excellent candidates to control and manipulate the polarization of light in optical devices. In nano-photonics, the self-assembly of colloidal plasmonic nanoparticles gives rise to strong resonances in the visible range and, when such organizations are chiral, strong chiroplasmonic effect can be observed. In the present work, we describe the optical properties of chiral artificial nano-photonic materials, *Goldhelices*, which are hierarchically organized by Grazing Incidence Spraying. These *Goldhelices* are made by plasmonic nanoparticles (gold) grafted onto helical templates made from silica nanohelices. A comparison of oriented vs non-oriented surfaces has been performed by Mueller matrix polarimetry, showing the importance of the organization of the *Goldhelices* regarding their interaction with light. Moreover, mono- *vs* multi-layers photonic films are created and the measured optical properties are discussed and compared to simulations.

KEYWORDS: Gold nanoparticles, Nanohelix, Chirality, Hierachical organization, Grazing Incidence Spraying, Mueller Matrix Polarimetry

Materials which are structured at the nanoscale have unique optical, electronic or mechanical properties different from their bulk counterpart. In the last 30 years, great progress has been made in the preparation of discrete inorganic nanostructures with controllable chemical compositions and morphologies. These nanoscale objects are extremely promising materials and can greatly impact many areas like coatings, electronics, biomedical implants, solar cells… Since the seminal experiments of L. Pasteur on sodium ammonium tartrate crystals in 1848,[1] different enantiomers of a chiral molecule are known to interact differently with right- and left-handed circularly polarized light. More recently, chirality has been studied not only at the molecular level but also at the nanometric and the macroscopic scales. The chemical, electromagnetic or optical properties of such objects can be directly modified by the chiral nature of their components and potentially be very useful in a large variety of applications like sensors, asymmetric catalysis or optics.[2,3] The key challenge here is to organize the individual chiral nanostructures into large well-controlled architectures with controlled composition, density, spacing and orientation and to investigate the cooperative or collective optical properties at large scale in order to create materials that can be easily handled at the macroscale. Only bottom-up nanofabrication processes can reach such a degree of organization at a large scale and at low costs. Anisotropic particles such as disk- or rod-like particles offer a promising toolbox for multiscale hierarchical organization.[4] A

number of strategies to assemble these nanoobjects are developed. The proposed strategies rely on physical approaches based on controlled evaporation or shear force (dip-coating, doctor blade coating, microfluidic, spraying…),[5,6,7,8,9] or on incorporation in matrices, for example by formation of lyotropic mineral liquid crystals or in polymer networks.[10,11,12,13]

In order to control the interaction between materials and light, they need to be structured on a length scale smaller than the wavelength of the exciting electromagnetic field, i.e. with a characteristic scale of tens of nanometers for the applications in the visible range.[14] We recently designed new nano-objects which possess chiroptical properties based on non-chiral gold nanoparticles (GNPs) grafted on chiral nano-templates.[15] These templates are silica chiral nanohelices obtained by the mineralization of self-assembled gemini-type dialkyl diammonium amphiphilic molecules with tartrate counterions with finely tuned morphologies at the nanometric scale.[16,17] These SiO_2@GNPs helices are named the *Goldhelices*[15] and show chiroptical activity values similar to the structures previously reported by GNPs assembled on organic templates like DNA or peptides.[14,18,19]

In this article, we demonstrate the chiroptical properties of thin films composed of hierarchically organized *Goldhelices* obtained by Grazing Incidence Spraying (GIS),[20,21,22,23] combined to the Layer-by-Layer (LbL) assembly approach (Scheme Figure 1).[24,25,26,27] The orientation of *Goldhelices* in the film, the average spacing and the distance between the layers are well-controlled. The thin films with linearly oriented vs randomly deposited *Goldhelices* as well as mono- *vs* multi-layers organization are

compared. Structure-dependent optical properties measured by Mueller Matrix Polarimetry (MMP) are finally discussed and compared to simulations.

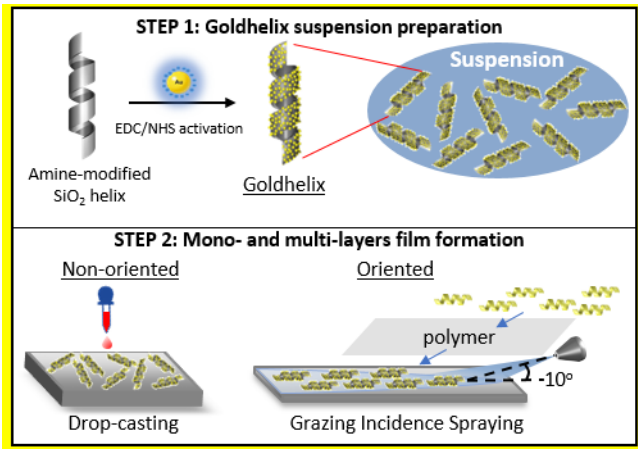

Figure 1. General scheme of the chiral photonic nanodevices buildup. Step 1: covalent grafting of the GNPs on the silica nanohelices to form the Goldhelix suspension in water. Step 2: Formation of non-oriented and oriented films by drop-casting and Grazing Incidence Spraying, both combined with the Layer-by-Layer approach to form the multilayers samples.

RESULTS AND DISCUSSION

1/ Presentation of the *Goldhelices*.

The building blocks used in the present study are nanometric silica twisted ribbons covered with 10 nm GNPs previously named as *Goldhelices*.[15] **Erreur ! Signet non défini.** Following the common rules in term of helicity nomenclature, the right-handed helices will be named P-helix (for Plus) and the left-handed M-helix (for Minus). The details of their synthesis are presented in the Supporting Information (SI-1). In our previous

report,[15] the interaction between the chiral silica template and the GNPs was electrostatic in nature which was not stable upon the variation of external parameters such as pH, ionic strength or the presence of organic solvent, but also unable to endure a shear flow and the drying of the samples. Here, we developed a system in which the carboxylic groups of the GNP ligands and the amine grafted on the silica surface are linked by covalent bonds via 1-Ethyl-3-(3-dimethylaminopropyl)carbodiimide (EDC) / N-hydroxysuccinimide (NHS) activation. As presented in Supporting Information, an optimization of the activation process conditions allowed creating homogeneous well-covered *Goldhelices*, without any impact of the drying step (SI-2 and Figure 2-a).

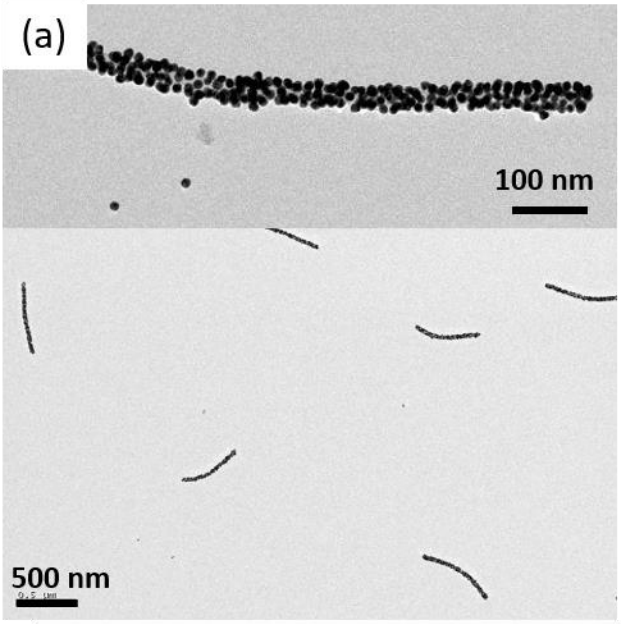
(a)
100 nm
500 nm

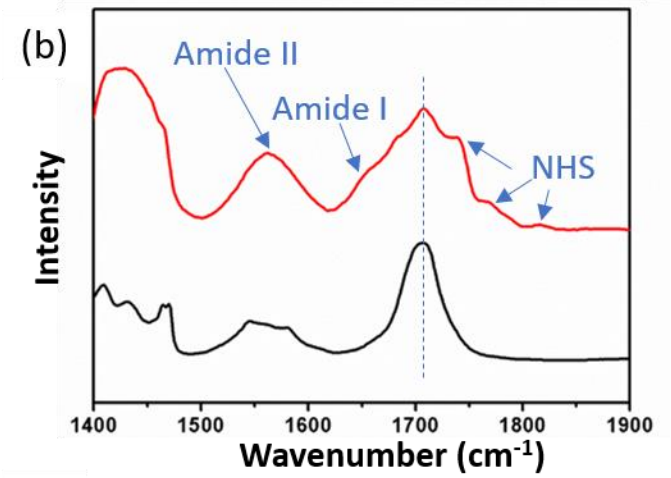
(b)
Amide II
Amide I
NHS
Intensity
1400
1500
1600
1700
1800
1900
Wavenumber (cm-1)

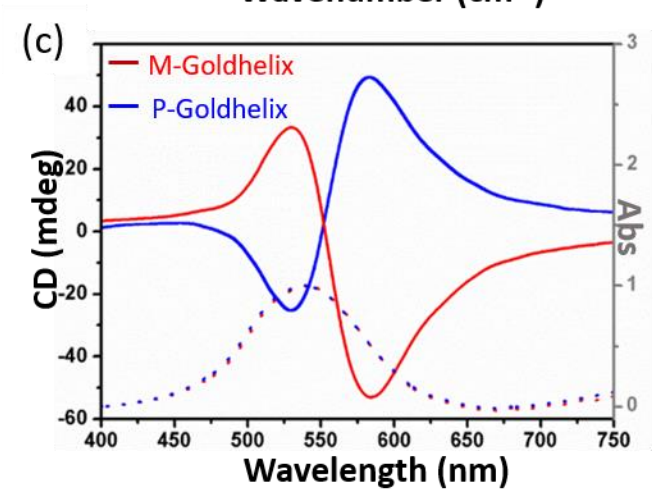
(c)
M-Goldhelix
P-Goldhelix
CD (mdeg)
Abs
40
20
0
-20
-40
-60
3
2
1
0
400
450
500
550
600
650
700
750
Wavelength (nm)

Figure 2. Goldhelices – (a) TEM images. (b) Infra-Red spectra of covalent (red) and electrostatic (black) Goldhelices. (c) Circular Dichroism (CD) (full line) and absorbance (dashed line) spectra of P- and M- Goldhelices suspensions in water.

The covalent bond between the carboxylic group of the GNPs and the silica-NH_2 surface has been confirmed by InfraRed spectroscopy (Figure 2-b). The black and red lines correspond to the electrostatic and covalent *Goldhelices*, respectively. It can be observed that in both cases, clear peaks at 1710 cm^{-1} are observed corresponding to the COOH groups of GNPs. A broad shoulder at 1650 cm^{-1} and a new peak at 1560 cm^{-1}, corresponding to the amide I and II vibration respectively, indicate the formation of covalent bonds between the GNPs and the silica aminated surface. The presence of the three peaks at 1740, 1760 and 1820 cm^{-1} is related to the COO stretching modes of the not reacting succinimide ester groups.[28,29,30] Finally, the electronic circular dichroism spectra of P- and M-*Goldhelices* in suspension in water show an opposite Cotton effect at the wavelength centered at around 550 nm (Figure 2-c). For a constant concentration in GNPs (spectra normalized by the absorbance at 550 nm), the CD of the covalent *Goldhelices* is much stronger than that of the electrostatic ones. The chiroptical properties calculated by the dimensionless Kuhn factor from the ellipticity θ (the so-called g-factor):[31]

$$g = \frac{\Delta A}{A} \approx \frac{4\times\theta(rad)}{\ln 10\times A} = \frac{4\pi\times\theta(mdeg)}{180\times 1000\times\ln 10\times A} = \frac{\theta}{32982A}, \quad (1)$$

showed that the g-factor for the covalent *Goldhelices* is 4.4 x 10^{-3} (g-factor of the electrostatic ones was 3.10^{-4}, i.e. ten times lower). ΔA is the difference between the

absorbance of left circularly polarized and right circularly polarized light. A is the absorbance measured with an unpolarized incident light.

2/ *Goldhelix* monolayer films

These *Goldhelices* can be dispersed in various solvents (water at different pH or organic solvents) and be dried while retaining the helix-structures and the helical organization of the GNPs. Therefore, they can be deposited on a surface to create thin films either with i) non-oriented *Goldhelices* by drop-casting or ii) oriented *Goldhelices* using the GIS technique.[20,21,22,23] For the *Goldhelices* deposition with GIS, their suspension in water is sprayed at a low angle (10°) on a glass slide coated with polyethyleneimine. The opposite charges between the negatively charged *Goldhelices* (zeta potential is -20 mV at pH 6) and the positively charged polymer on the substrate ensure the strong adsorption of the *Goldhelices* through electrostatic interactions, while the shear force of the flowing liquid induces the orientation of the helices. Figure 3 presents the SEM images of non-oriented (Figure 3a) and oriented *Goldhelix* films (Figure 3d). The nano-object densities both on the oriented and non-oriented surfaces were evaluated by UV-Vis absorption spectroscopy. In both cases, the UV-Vis absorption is around 0.6 at 550 nm and corresponds to a surface coverage of 22% as evaluated with Image J on SEM images. The distribution of orientation can be extracted and a 2D order parameter (S_{2D}) can be calculated and be used to characterize the degree of alignment: $S_{2D} = <2\cos^2\delta-1>$, where δ is the angle between each nanohelix principal axis and the spraying direction. The 2D order parameter $S_{2D} = 0$ corresponds to a random distribution of nanohelices (isotropic films) and $S_{2D} = 1$ corresponds to a perfectly parallel alignment ($\delta = 0°$, anisotropic film). Details of the orientation analysis are presented in Supporting Information (SI-3.). Figure

3 presents the SEM images of a non-oriented thin film and of an oriented monolayer (Figure 3-a, d) and the images color-coded according to the Goldhelices orientation (Figure 3-b, e). The orientation distribution can be extracted from the image analysis (Figure 3-c, f) and the corresponding 2D order parameter can be calculated. It appears clearly that the Goldhelices have no preferential orientation in the drop-casted sample (S_{2D} = 0.12), whereas the order parameter is much higher for the oriented monolayer (S_{2D} = 0.62), which corresponds to 67% of the Goldhelices oriented at ±25° from the spraying direction and 91% of the helices oriented at ±45°. One can observe on the SEM images (Figure 3-a, c) that individual GNPs are also present. These particles remained from the initial grafting because of the difficulty to remove all of them during the washing process. These individual GNPs do not affect the CD measurements but decrease the g-factor value as the UV-Vis absorbance value used for the normalization arises from both individual GNPs and GNPs from the Goldhelices.

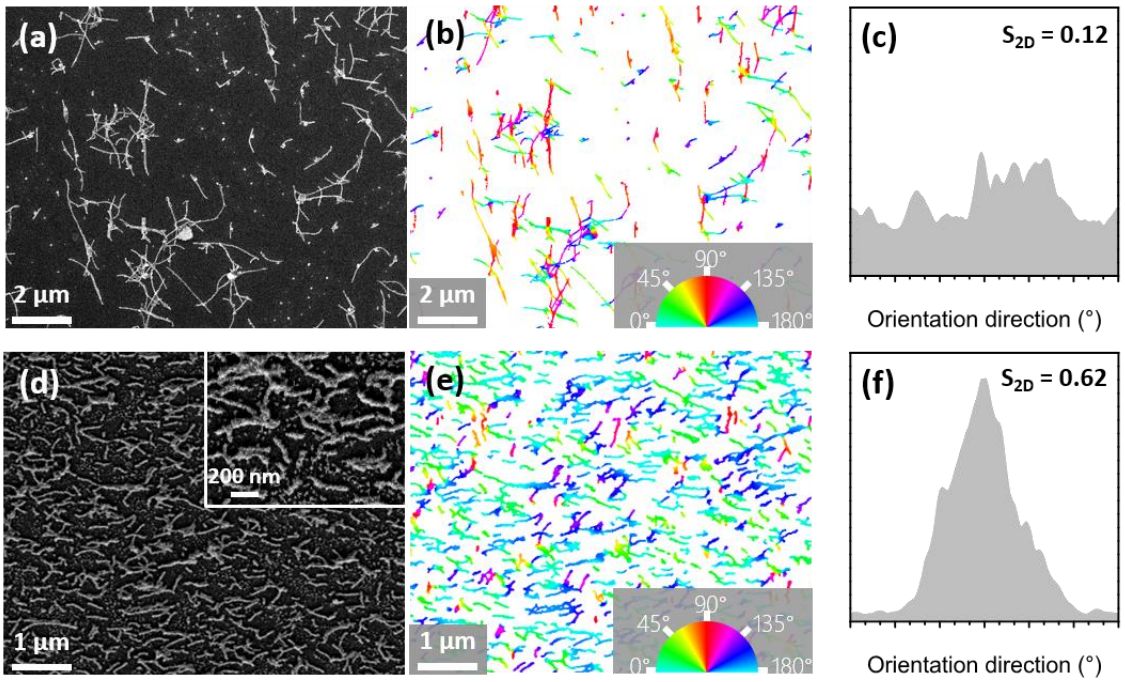

Figure 3- SEM images of a non-oriented thin film (a) and an oriented layer (d) of Goldhelices. Image analysis for the non-oriented (b) and the oriented (e) samples revealing the orientation of the objects. The Goldhelices are color-coded according to their orientation (the color scale is shown). The distribution of orientation with respect to the main direction and the corresponding nematic order parameter S_{2D} is extracted from the image analysis (c, f).

Optical properties of such 2D organized *Goldhelices* are evaluated by MMP by using a phase modulation ellipsometer, which only measures 12 elements of the Mueller matrix. Indeed, as this system only generates linear polarization, only the three first columns of the Mueller matrix are accessible. The other elements can be deduced by considering the symmetry of the Mueller matrix in a non-depolarizing structure.[32] MMP is a suitable tool to investigate the polarization state induced by arrangement of nanoparticles. As example, the Mueller matrix was used to characterize polarizer composed of aligned gold nanowires.[33] Brakstad *et al.*[34] have shown that the Brillouin Zone (BZ) boundaries of an array composed of GNPs can be directly imaged from the block-diagonal Mueller matrix elements. In addition, MMP has also been exploited to investigate the linear optical anisotropy in linear chain of GNPs and circular dichroism in curved nanoparticle chain.[35,36] According to Azzam *et al.*,[37] the linear dichroism (LD), linear birefringence (LB), circular dichroism (CD) and circular birefringence (CB) can be directly obtained from the measured Mueller matrix M according to the differential matrix decomposition: $L = \ln M$ with

$$L = \begin{bmatrix} 0 & -LD & -LD' & CD \\ -LD & 0 & CB & LB' \\ -LD' & -CB & 0 & -LB \\ CD & -LB' & LB & 0 \end{bmatrix}. \quad (2)$$

Here, LD and LB are the linear dichroism and birefringence set by the laboratory frame (Ox,Oy) which is fixed and the sample is rotated. In the case of aligned helix film, the helices are oriented along the Oy axis for an azimuth angle of 0°. LD' and LB' are the linear dichroism and birefringence along the ±45° axes. Figure 4 shows the Mueller matrices of a non-oriented (a) and an oriented (b) thin film of *M-Goldhelices*.

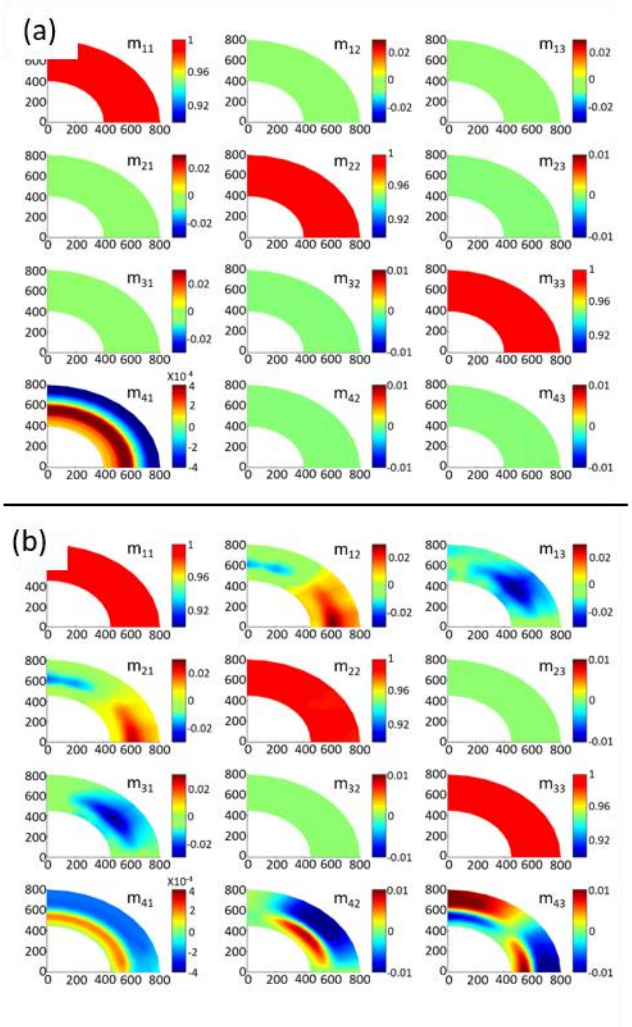

Figure 4- Partial Mueller matrix of M-Goldhelix non-oriented (a) and oriented (b) thin films. The radial coordinates are the wavelength in nm and the polar angle represents the sample azimuth angle.

The diagonal elements of the Mueller matrix of the non-oriented and oriented *Goldhelix* films, m_{11}, m_{22} and m_{33}, are close to 1. The measured off-diagonal elements of the Mueller matrix of the non-oriented *Goldhelix* film are equal to 0 except for m_{41}. Both films have similar m_{41} spectral variation. This parameter does not depend on the azimuth. This observation is coherent as this term, which is related to the CD, is invariant under sample rotation. On the contrary, films composed of oriented *Goldhelices* exhibit a more complex Mueller matrix. Only the m_{32} and m_{23} elements, associated to the CB, are equal to 0. The Mueller matrix elements of m_{12} and m_{21} (LD), m_{13} and m_{31} (LD'), m_{42} (LB') and m_{43} (LB) are all linear components of the polarization and depend on the sample orientation. The m_{12} and m_{13} elements are close to the m_{21} and m_{31} elements, respectively. The m_{12}, m_{21}, and m_{43} are close to 0 for an azimuth angle of 45° whereas for m_{13}, m_{31}, m_{42}, such angle was observed at 0° and 90°. Being related to the linear dichroism and linear birefringence, these terms reveal that the eigen linear polarization direction is parallel to the main helix axis and the orientation of the *Goldhelices* in the direction of 0°. Finally, as it is shown on Figures 4 and 5-a, m_{41} is two orders of magnitude smaller than m_{12} ($1{,}3.10^{-4}$ for the CD and $1{,}6.10^{-2}$ for the LD. We thus conclude that the LD prevails over the CD.

The spectral dependence of LD, LB and CD of the *M-Goldhelix* films, deduced from the measured Mueller matrix, are given in Figure 5. The film composed of aligned

Goldhelices also exhibits LD and LB. Note that the CB is smaller than our detection limit. The LD is maximized while the LB and CD change in sign close to the plasmon resonance of GNPs (Figure 5-a).

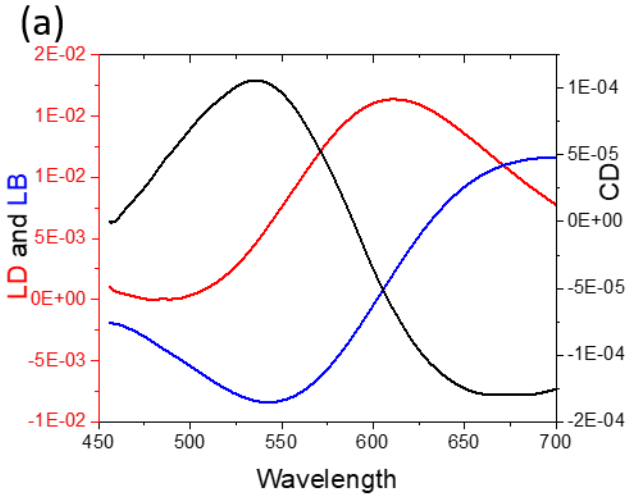
(a)
LD and LB
CD
Wavelength
2E-02
1E-02
1E-02
5E-03
0E+00
-5E-03
-1E-02
1E-04
5E-05
0E+00
-5E-05
-1E-04
-2E-04
450
500
550
600
650
700

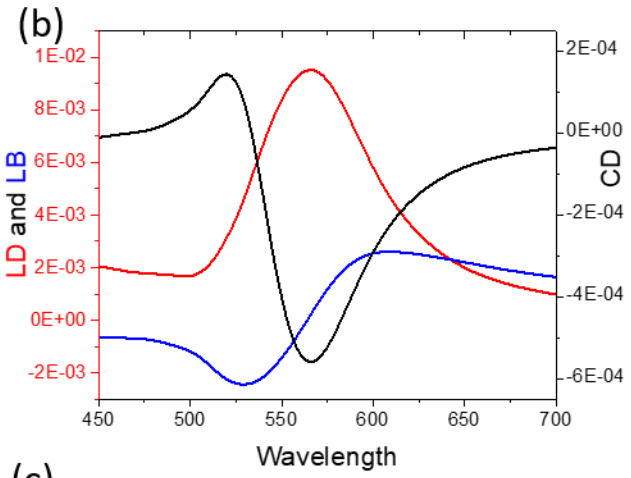
(b)
LD and LB
CD
Wavelength
1E-02
8E-03
6E-03
4E-03
2E-03
0E+00
-2E-03
2E-04
0E+00
-2E-04
-4E-04
-6E-04
450
500
550
600
650
700

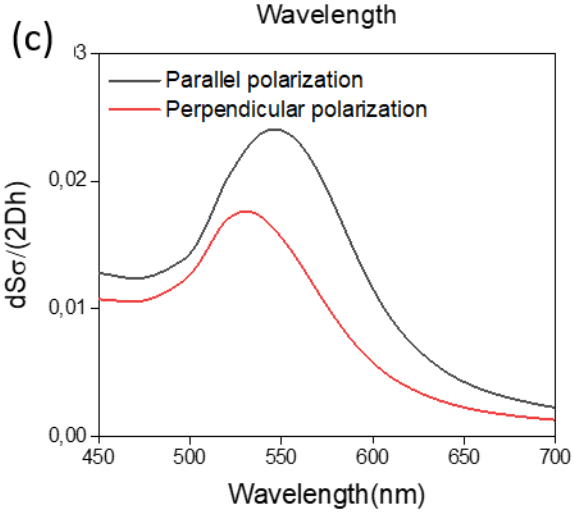
(c)
Parallel polarization
Perpendicular polarization
dSσ/(2Dh)
Wavelength(nm)
0,02
0,01
0,00
450
500
550
600
650
700

Figure 5- Measured (a) and simulated (b) LD, LB and CD of the oriented M-Goldhelix thin film. (c) Simulated transversal and longitudinal absorbance. The LD and LB spectra are given for an azimuth equals to 0°. The CD spectra are averaged over all azimuths.

Interestingly, the g-factors calculated from *Goldhelices* in suspension, non-oriented or oriented thin films are all the same order of magnitude, meaning that the alignment has no impact on the global chirality (g factors are $4.4\text{x}10^{-3}$, $4.3\text{x}10^{-3}$ and $4.3\text{x}10^{-3}$ respectively). Simulations based on coupled dipoles method (CDM) are proposed to investigate the provenance of CD, LD and LB. We consider a film composed of a monolayer of *Goldhelices*. By neglecting the interaction between *Goldhelices* and assuming monodispersed *Goldhelices* in length, the LD, LB and CD of the film can be calculated from:

$$LD = \frac{d}{2Dh}(\sigma_{\parallel} - \sigma_{\perp})S \qquad (3)$$

$$LB = \frac{d}{2Dh}(\varphi_{\parallel} - \varphi_{\perp})S \qquad (4)$$

$$CD = \frac{d}{2Dh}(\sigma_L - \sigma_R) \qquad (5)$$

where d, D and h are the surface density, the width and the length of a *Goldhelix*, respectively. S is the 2D nematic order parameter. $\sigma_{\parallel}$, $\sigma_{\perp}$, σ_R and σ_L are the extinction cross sections of a single *Goldhelix* calculated for a linear polarization parallel and perpendicular to the helix axis and for right and left-handed circular polarization, respectively. $\varphi_{\parallel}$ and $\varphi_{\perp}$ are the phase lag cross sections of a single *Goldhelix*, determined for a polarization parallel and perpendicular to the helix axis. Thus, this model takes into

account misalignment of *Goldhelices*. *S* is equal to 0 for films composed of randomly oriented helices. According to equations (3) and (4), such a non-oriented film cannot exhibit linear dichroism and birefringence. This result is in agreement with the Mueller matrix measurements. Since the CD does not depend on the *S* value (eq. (5)), the measured circular dichroism of randomly oriented *Goldhelix* film is similar to the measured one for oriented thin films as well as for the suspension. On the contrary, the LD and LB are maximized for a perfectly aligned *Goldhelix* thin film. As published previously and detailed in the SI-4,[15] the extinction and the phase-lag cross sections of a single *Goldhelix* are simulated according to the coupled dipole methods (CDM). As described in SI-4, each spherical nanoparticle is modeled as a point dipole. CDM takes into account the dipolar interaction between nanoparticles in the same helix. We neglect the interaction between the nanoparticles located on different helices. This model requires the knowledge of the nanoparticle sizes and positions. We assume that all nanoparticles have the same radius equal to 5 nm. Their positions are calculated as following: first, the nanoparticles are perfectly organized on a flat ribbon into a two-dimensional square lattice. The interparticle distance is 14 nm. Then, the ribbon is twisted with the geometrical parameters estimated by TEM (108 nm in pitch and 20 nm in width). The length of the Goldhelix is 520 nm. In this simulation, we consider that the nanoparticles are located in a homogeneous silica matrix. In other words, we neglect the interface between the silica helix and air where the nanoparticles are located. The simulated LD, CD and LB of the oriented *Goldhelix* film shown in Figure 5-b are in good agreement with the measured spectra. Indeed, the LD is maximized close to the plasmon resonance of GNPs while the LB and CD are bisignate spectra. This CD signal was also reported by

Kuzyk *et al.*[38] and Schreiber *et al.*[39] for Goldhelix perpendicular to the incident light. The CDM model, which only takes into account the organization of nanoparticles and the dipolar interactions, allows reproducing the measured CD spectra. The measured and simulated CD spectra change in sign by changing the helicity. This suggests that CD is related to dipolar interactions in chiral arrangement of nanoparticles. The measured spectra are broader than the simulated ones. In addition, a blue shift is observed on the simulations compared to the experimental spectra. These discrepancies can be explained by the fact that i) the simulations do not take into account the size distribution and the random position of GNPs (as discussed previously[15]), and the positional disorder as well as the nanoparticle size distribution can lead to an inhomogeneous broadening of the plasmon band, and ii) the emergence of interactions between the different *Goldhelices* when organized in oriented and non-oriented films. Indeed, it can be noted that the CD signal position of the simulated data corresponds to the Goldhelices in suspension result. Moreover, such a blue shift has already been observed with α-helix polypeptide thin films.[40] Finaly, the refractive index of the matrix chosen for the simulation is 1.45 (corresponding to a silica matrix) whereas the actual surrounding is a more complex medium as the nanoparticles are located at an interface between the silica helix and a mixture of air and the polymer used for GIS deposition. The sign of the CD depends on the chirality of the individual helix. In the case of the spectrum shown in Figure 5-b, it corresponds to a *M-Goldhelix* film suggesting that the CD comes from the chiral dipolar interaction between GNPs. Indeed, this film exhibits the same Mueller matrix that the one of the *P-Goldhelix* film except that the m_{41} element has an opposite sign. On the other hand, the LD and LB does not depend on the chirality, suggesting that these signals come

from the anisotropic coupling between gold nanoparticles in the one-dimensional structure. Indeed, as shown in Figure 5-c, *Goldhelices* exhibit two plasmon modes: the transversal (T-SPR) and the longitudinal (L-SPR) plasmon modes centered at 530 nm and 547 nm, respectively. The L-SPR and the T-SPR can be selectively excited by a linearly polarized light parallel and perpendicular to the *Goldhelix* axis. Thus, the LD and LB appearance in the oriented sample reveals a double interaction within the helices: along the eigen axes and following the curvature. Thus, *Goldhelix* films exhibit multiple anisotropies. To evaluate the main effect of the film on the polarization of light, we define the following anisotropic coefficients:

$$\alpha = \frac{LD^2}{LD^2+LD'^2+CD^2} \qquad (6)$$

$$\beta = \frac{LD'^2}{LD^2+LD'^2+CD^2} \qquad (7)$$

$$\gamma = \frac{CD^2}{LD^2+LD'^2+CD^2} \qquad (8)$$

The anisotropic coefficients can be viewed as the relative proportion of horizontal linear anisotropy (α), 45° linear anisotropy (β) or circular anisotropy (γ) of the film. These coefficients respect the following sum rules $\alpha + \beta + \gamma = 1$. Thus, the anisotropic coefficients of the films measured for each wavelength and azimuth angle can be represented in a ternary plot (Figure 6). All measurements are located close to γ = 1 for the non-oriented *Goldhelix* film, confirming that this film only exhibits circular dichroism. In other words, unpolarized light which passes through this film tends to be circularly polarized. On the contrary, the coefficient γ of aligned *Goldhelix* film is negligible

compared to α and β. Unpolarized light which passes through this film tends to be linearly polarized. We conclude that *Goldhelices* can be used as a building block for circular or linear polarizer. The evaluation of transmission losses is crucial for polarization state generators. As shown in SI-5, the measured transmittance is minimal in the 530-620 nm range, i.e. at the plasmon resonance of *Goldhelices*. The transmittance of a single layer is higher than 96%. Nevertheless, the CD and LD values that can be reached with these monolayer *Goldhelix* films are relatively low. We then evaluate the effect of having the multilayer of *Goldhelix* films on their chiroptical properties.

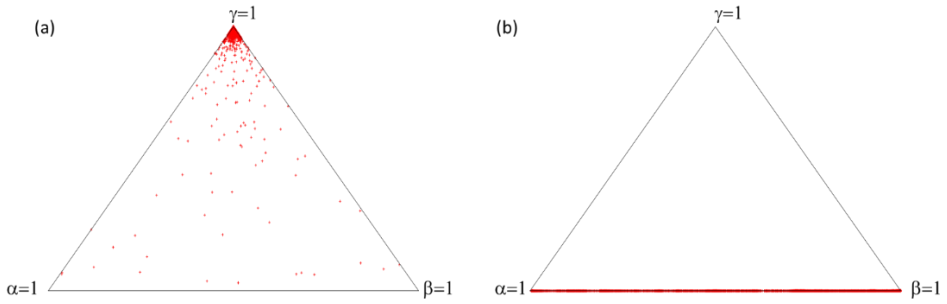

Figure 6- Anisotropic coefficients for each wavelength and azimuth angle for the non-oriented (a) and oriented (b) Goldhelix films.

3/ Multilayer *Goldhelices*: dense deposition

In order to increase the local concentration of *Goldhelices*, multilayer depositions were performed. Again, non-oriented vs oriented films were compared, the former by repeating the drop-casting of the suspension (4 times) on the same substrate. For the oriented sample, a high density of *Goldhelices* on the surface cannot be obtained by longer spraying time because the helices can only be deposited on a positively charged surface

and not as an ad-layer on top of already adsorbed helices due to the electrostatic repulsion between similarly charged helices. However, by spraying a PEI monolayer (thickness ~ 1 nm), it was possible to further deposit *Goldhelices*. This alternate deposition process was repeated three times, forming a thin film whose structure is noted as SiO_2/(PEI/Goldhelices)$_3$ (See the scheme of the process in Figure 7).

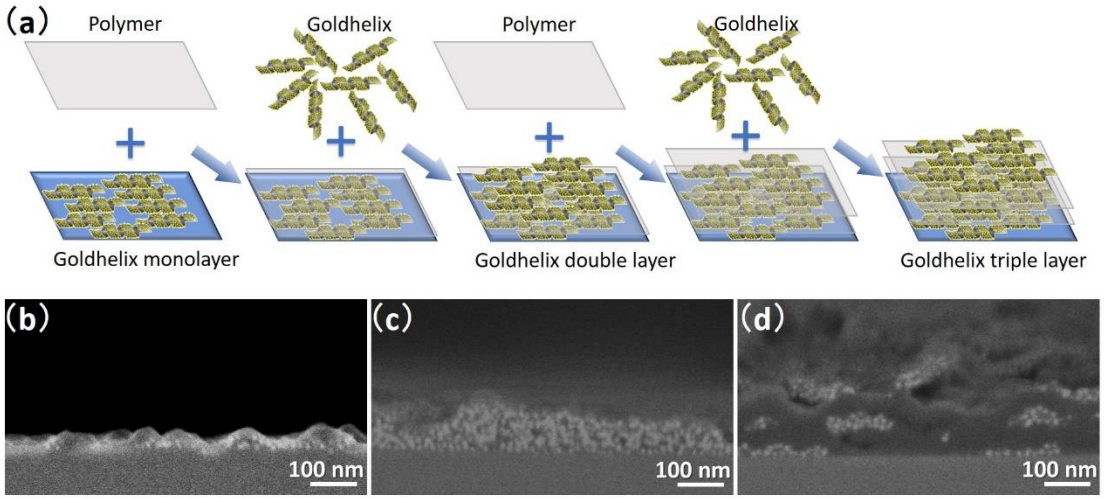

Figure 7- (a) Scheme of the GIS and LbL combined techniques for the creation of Goldhelix multilayer films. Cross-section (b-d) SEM images of a monolayer film (b), a triple layer film with a single PEI deposition between the Goldhelices layers (c) and a triple layer film with a polyelectrolyte multilayer (PEI/(PSS/PAH)$_{15}$/PSS/PEI, thickness = 56 nm) between the Golhelices layers (d).

The spacing between the *Goldhelix* layers can be conveniently varied by using polyelectrolyte multilayers assembled by the Layer-by-Layer (LbL) approach. The repeated alternated adsorption of negatively and positively charged polyelectrolytes (polystyrene sulfonate (PSS) and polyallylamine hydrochloride (PAH) respectively)

allows tuning the spacing between the *Goldhelix* layers with a nm-scale resolution, i.e. three oriented *Goldhelix* layers were deposited separated by a polyelectrolyte multilayer (PEM) spacer. The structure of the thin films can thus be noted as SiO_2/PEI/Goldhelices/(PEM/Goldhelices)$_2$ with PEM = PEI, PEI/(PSS/PAH)$_5$/PSS/PEI or PEI/(PSS/PAH)$_{15}$/PSS/PEI. The Figures 7-b-d show cross sections of (b) a monolayer film, (c) a multilayer film separated by one layer of polymer corresponding to ~1 nm spacer, and (d) a multilayer film separated by 15 layer pairs of polymer corresponding to ~56 nm spacer. The thickness of 1 nm given for a single PEI layer is extrapolated from measurements by ellipsometry on a flat substrate. The actual separation between neighboring Goldhelices is probably slightly different from this value as the conformation of the polymer on a non-homogeneously charged surface is different than on a flat substrate, but it is definitely smaller than the polymer thicknesses evaluated from the cross-section SEM images for the Goldhelices separated by polyelectrolyte multilayers, which are in good agreement with previously reported thicknesses.[41]

The maximum LD and g-factor values extracted for all the samples (monolayers and multilayers, non-oriented and aligned) measured by the Mueller matrices are summarized in Table 1. All these measurements have been done on *M-Goldhelix* films.

Sample	**Non-oriented**				**Oriented**			
	Suspension	Monolayer	Multilayers		Monolayer	Multilayers (3 layers)		
			Gap			Gap		
			0 nm	56 nm		1 nm	22 nm	56 nm
LD	0	0	0	0	0.038	0.051	0.035	0.045
g-factor (x10^{-3})	4.4	4.3	0	3.7	4.3	1.3	1.8	4.4

Table 1- LD and g-factor values of samples with or without orientation, with mono- or multi-layers with different gaps between the layers.

As expected, all the samples prepared by GIS show linear dichroism due to the highly oriented *Goldhelices* whereas the non-oriented ones do not. This confirms the preferential orientation observed in SEM but also the coupling between the GNPs along the helix main axis. Regarding the *Goldhelices* in suspension and on monolayer, they show the similar g-factors regardless of their orientation, confirming that the circular dichroism of the sample is determined by the individual *Goldhelix*, and is not dependent on the drying or the alignment of the samples. On the other hand, it is interesting to note that the g-factors decrease strongly for the *Goldhelix* layers without spacer or with 1 nm polymer spacer. The g-factor is 0 for the non-oriented sample and 1.3×10^{-3} for the oriented multilayers with a 1 nm polymer spacer. This may be because when the spacer between the *Goldhelix* films is on the order of the distances between the GNPs, the GNPs do not only interact with the other GNPs of the same helix but also with the GNPs grafted on the neighboring *Goldhelices* (Figure 8). The chiral character given by the helical template is thus lost, which results in the disappearance of the chiroptical activity. When the spacer thickness is increased, in both oriented and non-oriented multilayer films, the chiroptical activity (3.7×10^{-3} for non-oriented and 4.4×10^{-3} for oriented) becomes similar to that of the monolayer and of the suspension recovering the individual chiral character of the *Goldhelices*.

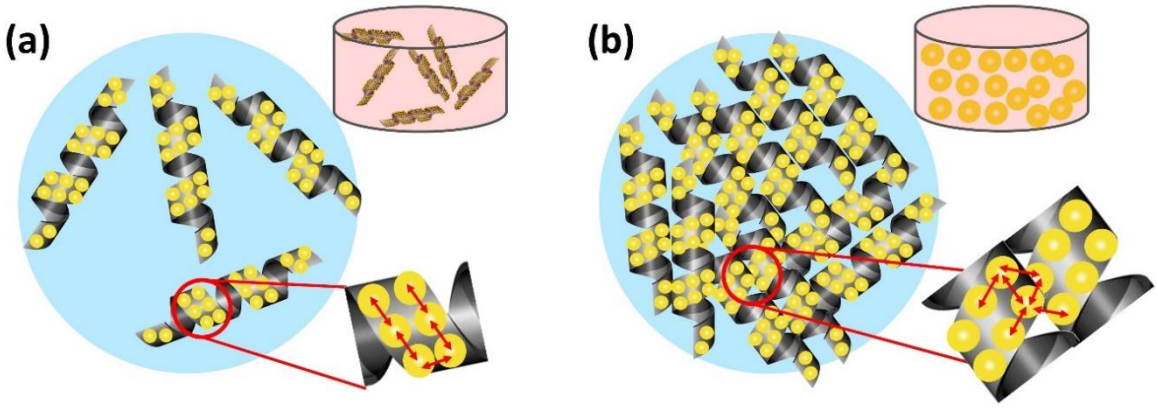

Figure 8- Scheme of the GNPs interactions when they are isolated the ones from the other ones (a) or in contact the ones with the other ones (b). In the first case the GNPs interact only with their Goldhelix neighbor whereas in the second case they can interact with the GNPs of the other Goldhelices, losing the chiral character of the interaction and giving an optical signal close to the one which would be obtained from a homogeneous suspension of GNPs.

Previously in this article, we have shown that unpolarized light which passes through the *Goldhelix* films tends to be circularly or linearly polarized for non-oriented and oriented samples respectively. The formation of multilayer *Goldhelix* films should tend to perfect polarizers. If the optical properties are not altered by the layers formation, one can wonder the number of layers needed to create perfect polarizers. As developed in the Supporting Information (SI-6), in the case of the oriented sample, the polarization of light after passing through the polarizer would be systematically linearly polarized whatever the polarization state of the incident light if it passes through 100 *Goldhelix* layers. This multilayer would be considered as a "perfect polarizer". In the case of the non-oriented samples, a perfect circular polarizer would need more than 1000 layers. Even if the number of layers for the creation of the linear polarizer could be doable, the light

absorbance of such samples in both oriented and non-oriented samples would probably be very high decreasing its capacity of being a perfect polarizer.

CONCLUSION:

In conclusion, we have developed a simple and efficient way to tune the optical properties of hierarchically organized *Goldhelix* films, using as building blocks *Goldhelices* previously settled by us.[15] Here we have further developed the fabrication method by grafting gold plasmonic nanoparticles on the silica helices with covalent bonds. These new covalent *Goldhelices* can be dispersed in various solvents and can withstand the drying of the samples without any damage to the structure retaining the chiroptical properties of the nanoobjects. Therefore, they could be organized on surfaces via Grazing Incidence Spraying (GIS). A comparison of oriented vs non-oriented thin films has been performed using Mueller matrix polarimetry measurements, showing the importance of the linear and circular anisotropies regarding the interaction with light. The non-oriented sample shows a circular polarization without linear dichroism/birefringence whereas the oriented ones show linear polarization of light which becomes dominant. We then used the Layer-by-Layer deposition approach to perform multilayer deposition. The optical properties of these multilayers were also strongly dependent on the polyelectrolyte spacer thickness between the different *Goldhelix* layers. When the spacer thickness is on the order of 50 nm, the chiroptical property of the multilayer film was similar to that of the monolayer film or the suspension, whereas when the spacer thickness is close to the GNP-GNP distance, we observed the disappearance of the chiroptical property (while maintaining the linear dichroism at the same order of magnitude) likely due to the interlayer interaction. While such thin films would probably not be used as perfect

polarizers because of the high number of layers needed, we clearly demonstrated that it is possible to control the optical properties based on building block nanostructure, *Goldhelix*, via its hierarchical organization.

METHODS SECTION:

Synthesis of Gemini Tartrate and Gel Formation. The 16-2-16 amphiphiles with tartrate counterions were synthesized according to previously published data. To make the organic gel, 3.58 mg of the 16-2-16 L or D-tartrate powder were dissolved into 5 mL of Milli-Q water to obtain a concentration of 1 mM 16-2-16 tartrate. The solutions were then heated up to 60 °C (above the Krafft temperature which is 43 °C for 16-2-16 tartrate at 10 mM) for 20 min for a complete dissolution and incubated at 20 °C. At the concentration of 1 mM, twisted ribbons were observed after 1 h at 20 °C, until they transform to helical ribbons after 1 day. For the experiments performed in this paper, only twist ribbons were used. Both are denominated under the generic name Nanohelices.

Preparation of Silica Nanohelices and their surface modification. These organic self-assemblies are used as templates to prepare silica nanostructures through a sol−gel transcription procedure.[Erreur ! Signet non défini.] In a typical preparation, 500 μL of tetraethoxysilane (TEOS) were added to 10 mL of 0.1 mM aqueous solution of L-tartaric acid (pH 3.8) and prehydrolyzed at 20 °C by stirring on the roller-mixer for 7 h. In parallel, a solution of 1 mM 16-2-16 gemini surfactant with L-tartrate counterion was aged for 2 h for the formation of the twisted nanoribbons. Equal volumes of prehydrolyzed TEOS in 0.1 mM aqueous solution of tartaric acid and organic gels were

mixed (typically, 2 mL of each) and stirred at 20 °C with a roller-mixer overnight. Once the transcription was completed, the mixture was washed thoroughly with isopropanol, in order to solubilize the organic byproducts and eliminate the excess of TEOS (washing 5 times with isopropanol by centrifugation (5 min, 2000 G) and re-dispersing in isopropanol). Basically, from 3.6 mg of organic gel, we obtained 3.5 mg of silica nanohelices. The silica nanohelices were then functionalized via a surface chemical modification with (3-aminopropyl) triethoxysilane (APTES) as previously developped.[Erreur ! Signet non défini.] Generally, 25 μmol of APTES were added per 0.5 mg of silica nanohelices in ethanol. The reaction mixture was submitted to ultrasonication for 5 min and then kept in an oil bath overnight at 80 °C, followed by five times washing by centrifugation in absolute ethanol. This modification procedure can be repeated once to improve the coverage of the silica surface with amine groups.

Synthesis of GNPs and surface ligands exchange. The GNPs were synthesized using both tannic acid and trisodium citrate as reducing and capping agents following a previously optimized procedure.[Erreur ! Signet non défini.] To make 100 mL of a GNP suspension, two stock solutions were prepared: Solution A: 1 mL of 1% aqueous gold chloride in 80 mL of ultra-pure water and Solution B: 4 mL of 1% trisodium citrate·$2H_2O$ in 16 mL of ultra-pure water, to which 0.1 mL of 1% tannic acid was added. After solution A and solution B were kept at 60 °C for 15 min, the two solutions were mixed into one flask and heated up to 100 °C under reflux for 1h and cooled in ice bath. 10 nm GNPs stabilized with tannic acid and tri-sodium citrate mixture ligands are formed. This GNPs stabilizers exchange was done by using O-(2-Carboxyethyl)-O'-(2-mercaptoethyl) heptaethylene glycol (noted as PEG). In a typical preparation process, 8mL of as-

synthesized GNPs were centrifuged at 21000G for 30 min, followed by removing 6 mL of supernatant. Then, 2 mL of a 10 mM solution of PEG in ethanol was added. The solution was sonicated for 10 min and placed on a shaker at 400 rpm overnight at 4°C. The mixture was washed three times by centrifugation and redispersed with ultra-pure water.

Synthesis of *Goldhelices*: To create a covalent bond between GNPs and NH_2 modified silica helices, the activation of the COOH groups stabilizing the GNPs is required.[42] 12mM EDC (1-ethyl-3-(3-dimethylaminopropyl)carbodiimide hydrochloride) and 60mM NHS (N-hydroxysuccinimide) solution was used. First, the aqueous solution of 12mM EDC and 60mM NHS was aged for 5 hours under 4 ^{o}C and then used to activate the GNP ligands (volume ratio GNPs / EDC/NHS mixture is 1:1). The concentration of GNPs suspension is 16 times higher than the as-synthesized GNPs suspension. The mixture was shaken on a plate shaker at 400 rpm during 6h at 4°C. The activated GNPs were then washed with water by centrifugation. In a second time, 50µL of 0.6 mg/mL nanohelices-NH_2 was added to 0.5mL of activated GNPs. The mixture was then placed in a sonication bath 10 min and transferred on the shaker plate at 400 rpm for at least one day at 20°C. The samples were then washed 5 times with ultra-pure water by centrifugation (15 min, 2000 G), until the supernatant remains transparent.

Helices alignment by Grazing Incidence Spraying. Very dilute suspensions (5 mg/L) of *Goldhelices* were sprayed at an angle of 10° on a substrate coated with poly(ethyleneimine) (PEI). The GIS setup is a home-made computer-controlled setup in which the air flow (30 L/min), liquid flow (1 mL/min), angle (10°) and distance (0.5 cm) between the Spray Nozzle (Aztek A480 airbrush, internal diameter: 1.03 mm) and

substrate can be precisely controlled. The substrates were glass slides which were previously cleaned using a 2 % (V/V) Hellmanex solution followed by rinsing in ethanol and ultra-pure water. The substrates were plasma activated for 30 s and subsequently coated with a PEI anchoring layer deposited by spraying an aqueous PEI solution ($M_n \approx$ 60 000 g.mol^{-1}, 2.5 mg/mL) for 6 s followed by water-rinsing for 10 s using air-pump spray cans and drying with a nitrogen flow.

The multilayer samples have been prepared by spraying the polymer solutions for 6 seconds followed by water-rinsing for 10 s using air-pump spray cans for the PEI layers and a home-made spraying robot for the poly(sodium 4-styrenesulfonate) (PSS) and poly(allylamine hydrochloride) (PAH) layers before drying with a nitrogen flow. PSS ($M_w \approx$ 70 000 g.mol^{-1}, 0.62 mg/mL) and PAH ($M_w \approx$ 15 000 g.mol^{-1}, 0.29 mg/mL) were dissolved in a 0.5 M NaCl solution. The deposition sequence that we have used in this study can be noted as SiO_2/(PEI/Goldhelices)$_3$ for the multilayer sample with a 1 nm polymer spacer between the Goldhelices layers and SiO_2/PEI/Golhelices/(PEI/(PSS/PAH)$_x$/PSS/PEI/Golhelices)$_2$ with x = 5 or 15 for the multilayer samples with a 22 and 56 nm polymer spacer respectively.

Characterization of materials:

Electronic Circular Dichroism (ECD) spectra were recorded on a Jasco J-815 CD spectrometer. The scan rate was 50 nm/min, accumulation was set to 10. All CD experiments were carried out in ultra-pure water (pH = 6.0 ± 0.1) with a quartz cuvette (10 mm path length) at 25 °C.

Mueller Matrix Polarimetry was measured in transmission at a normal incidence by using two ellipsometers: a homemade dual rotating compensator ellipsometer[43] and a phase modulation ellipsometer (UVISEL, Horiba). The first ellipsometer measures all elements of the Mueller matrix. However, it has a smaller sensitivity than the phase modulation ellipsometer and it is only used to confirm that the film does not exhibit depolarization effects. The phase modulation ellipsometer only measures 12 elements of the Mueller matrix. Indeed, as this instrument only generates linear polarization, only the first three columns of the Mueller matrix are accessible. The other elements can be deduced by considering the symmetry of the Mueller matrix in non-depolarizing structure.[44] The Mueller matrix is recorded in the 455 nm-795 nm spectral range for several sample azimuths.

Transmission Electron Microscopy was performed with a Philips EM 120 electron microscope operating at 120 kV, and the images were collected by 2k × 2k Gatan ssCCD camera. Drops of diluted dispersions of the hybrids were deposited on carbon film coated 200/400-mesh copper grids.

Scanning Electron Miscroscopy: Cross-section of the samples have been performed with a Hitachi IM4000Plus ion milling system. A low-energy Ar^+ ion beam (6 keV) is used to produce a polished and undistorted cross-section without applying mechanical stress to the sample. The cross-section was observed using a FEG-SEM (Hitachi SU8010) at 1 keV. The images were taken with the SE-in lens detector. The plane view of the sample was imaged using a FEG-SEM (Zeiss GeminiSEM 500) at 1 kV with a Everhart-Thornley SE detector.

Images have been analyzed by ImageJ with the plugin OrientationJ.[45,46,47] This technique is based on the analysis of the structure tensor in a local neighborhood and the orientation direction was determined for each pixel on the images.

ASSOCIATED CONTENT

Supporting Information. SI-1: Different steps of the formation of the helices and electrostatic *Goldhelices*. SI -2: Optimization of the GNPs covalent grafting. SI-3: Detailed orientation analysis of the SEM images. SI-4: CDM modelization of the *Goldhelices*. SI-5: Transmittance spectra of a single layer of *Goldhelix*. SI-6: Number of *Goldhelix* layers to create perfect polarizers

AUTHOR INFORMATION

Corresponding Author

* Emilie POUGET: e.pouget@cbmn.u-bordeaux.fr

* Yann BATTIE: yann.battie@univ-lorraine.fr

* Matthias PAULY: matthias.pauly@ics-cnrs.unistra.fr

Present Addresses

†If an author's address is different than the one given in the affiliation line, this information may be included here.

Author Contributions

The manuscript was written through contributions of all authors. All authors have given approval to the final version of the manuscript.

Funding Sources

JG and WW are supported by the Chinese Scholarship Council. JG is supported by the LabEx AMADEus (ANR-10-LABX-42) in the framework of IdEx Bordeaux (ANR-10-IDEX-03-02), *i.e.* the Investissements d'Avenir program of the French government managed by the Agence Nationale de la Recherche. VL is supported by the LabEx CSC "Chemistry of Complex Systems" (10-LABX-0026) in the framework of IdEx (ANR-10-IDEX-02-02).

Notes

Any additional relevant notes should be placed here.

ABBREVIATIONS

Grazing Incidence Spraying (GIS); gold nanoparticles (GNPs); Layer-by-Layer (LbL); Mueller Matrix Polarimetry (MMP); 1-Ethyl-3-(3-dimethylaminopropyl)carbodiimide (EDC); N-hydroxysuccinimide (NHS); Tetraethoxysilane (TEOS); (3-aminopropyl) triethoxysilane (APTES)

AKNOWLEDGMENT: We thank the Ellipsometry core facility of LCP-A2MC (Université de Lorraine - http://lcp-a2mc.univ-lorraine.fr). We thank the IECB microscopy platform and the IECB Chirality platform for the TEM and ECD

measurements. The authors thank Marc Schmutz from the Electron Microscopy Platform of the Institut Charles Sadron (Strasbourg, France) for SEM measurements.

TOC:

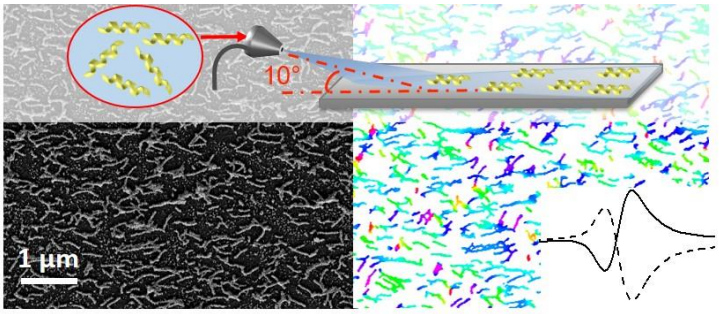

REFERENCES:

[1] Pasteur, M. L. Recherches Sur Les Relations Qui Peuvent Exister Entre La Forme Cristalline, La Composition Chimique Et Le Sens De La Polarisation Rotatoire. *Ann. Chim. Phys*. **1848**, *24*, 442-459.

[2] Wang, Y.; Xu, J.; Wang, Y.; Chen, H. Emerging Chirality in Nanoscience. *Chem. Soc. Rev.* **2013**, *42*, 2930-2962.

[3] Zhang, L.; Wang, T.; Shen, Z.; Liu, M. Chiral Nanoarchitectonics: Towards the Design, Self-Assembly, and Function of Nanoscale Chiral Twists and Helices. *Adv. Mater.* **2016**, *28(5)*, 1044-1059.

[4] Huang, Y.; Sasano, T.; Tsujii, Y.; Ohno, K. Well-Defined Polymer-Brush-Coated Rod-Shaped Particles: Synthesis and Formation of Liquid Crystals. *Macromolecules* **2016**, *49(22)*, 8430-8439.

[5] Leng, J.; Salmon J.-B. Microfluidic Crystallization. *Lab on a Chip* **2009**, *9*, 24-34.

[6] Leng, J. Drying of A Colloidal Suspension in Confined Geometry. *Phys. Rev. E* **2010**, *82*, 021405.

[7] Yang, H.; Jiang P. Large-Scale Colloidal Self-Assembly by Doctor Blade Coating. *Langmuir* **2010**, *26(16)*, 13173-13182.

[8] Brinker, C. J.; Hurd, A. J.; Schunk, P. R.; Frye, G. C.; Ashley, C. S. Review of Sol-Gel Thin Film Formation. *J. Non-Cryst. Solids* **1992**, *147&148*, 424-436.

[9] Gao, J. ; Semlali, S. ; Hunel, J. ; Montero, D. ; Battie, Y. ; Gonzalez-Rodriguez, D. ; Oda, R. ; Drisko, G. L. ; Pouget, E. ; Creating Regular Matrices of Aligned Silica Nanohelices: Theory and Realization, *Chem. Mater*. **2019**, DOI: 10.1021/acs.chemmater.9b04372

[10] Paul, D. R.; Robeson L. M. Polymer Nanotechnology: Nanocomposites. *Polymer* **2008**, *49(15)*, 3187-3204.

[11] Kumar, S. K.; Krishnamoorti, R. Nanocomposites: Structure, Phase Behavior, and Properties. *Annu. Rev. Chem. Biomol. Eng.* **2010**, *1*, 37-58.

[12] Sonin, A. S.; Churochkina, N. A.; Kaznacheev, A. V.; Golovanov, A. V. Mineral Liquid Crystal. *Colloid J.* **2017**, *79(4)*, 421-450.

[13] Vis, M.; Wensink, H. H. ; Lekkerkerker, H. N. W.; Kleshchanok, D.; Nematic and lamellar liquid-crystalline phases in suspensions of charged silica-coated gibbsite platelets. *Molecular Physics* **2015**, 113 (9-10), 1053-1060

[14] Schreiber, R.; Luong, N.; Fan Z.; Kuzyk, A.; Nickels, P. C.; Zhang, T.; Smith, D. M.; Yurke, B.; Kuang, W.; Govorov A. O.; Liedl, T. Chiral Plasmonic DNA Nanostructures with Switchable Circular Dichroism. *Nature Comm.* **2013**, *4*, 2948.

[15] Cheng, J.; Le Saux, G.; Gao, J.; Buffeteau, T.; Battie, Y.; Barois, P.; Ponsinet, V.; Delville, M.-H.; Ersen, O.; Pouget, E.; Oda, R. GoldHelix: Gold Nanoparticles Forming 3D Helical Superstructures with Controlled Morphology and Strong Chiroptical Property. *ACS Nano **2017**, 11 (4)*, 3806-3818.

[16] Delclos, T.; Aimé, C.; Pouget, E.; Brizard, A.; Huc, I.; Delville, M.-H.; Oda, R. Individualized Silica Nanohelices and Nanotubes: Tuning Inorganic Nanostructures Using Lipidic Self-assemblies. *Nano Lett.* **2008**, *8*, 1929-1935.

[17] Okazaki, Y.; Cheng, J.; Dedovets, D.; Kemper, G.; Delville, M.-H.; Durrieu, M.-C.; Ihara, H.; Takafuji, M.; Pouget, E.; Oda, R. Chiral Colloids: Homogeneous Suspension of Individualized SiO_2 Helical and Twisted Nanoribbons. *ACS Nano* **2014**, *8*, 6863-6872.

[18] Song, C; Blaber, M. G.; Zhao, G.; Zhang, P.; Fry, H. C.; Schatz, G. C.; Rosi, N. L. Tailorable Plasmonic Circular Dichroism Properties of Helical Nanoparticle Superstructures. *Nano Lett.* **2013**,*13(7)*, 3256-3261.

[19] Lan, X.; Liu, T.; Wang, Z.; Govorov, A. O.; Yan, H.; Liu, Y.; DNA-Guided Plasmonic Helix with Switchable Chirality, *J. Am. Chem. Soc.* **2018**, 140, 37, 11763-11770.

[20] Sekar, S.; Lemaire, V.; Hu, H.; Decher, G.; Pauly, M. Anisotropic optical and Conductive Properties of Oriented 1D-Nanoparticle Thin Films Made by Spray-assisted Self-assembly. *Faraday Discuss.* **2016**, *191*, 373-389.

[21] Blell, R.; Lin, X.; Lindström, T.; Ankerfors, M.; Pauly, M.; Felix, O.; Decher, G. Generating in-Plane Orientational Order in Multilayer Films Prepared by Spray-Assisted Layer-by-Layer Assembly. *ACS Nano* **2017**, *11(1)*, 84-94.

[22] Hu, H.; Pauly, M.; Felix, O.; Decher, G. Spray-assisted Alignment of Layer-by-Layer Assembled Silver Nanowires: A General Approach for The Preparation of Highly Anisotropic Nano-composite films. *Nanoscale* **2017**, *9(3)*, 1307-1314.

[23] Probst, P. T.; Sekar, S.; König, T. A. F.; Formanek, P.; Decher, G.; Fery, A.; Pauly, M. Highly Oriented Nanowire Thin Films with Anisotropic Optical Properties Driven by the Simultaneous Influence of Surface Templating and Shear Forces. *ACS Appl. Mater. Interfaces* **2018**, *10(3)*, 3046-3057.

[24] Decher, G. Fuzzy Nanoassemblies: Toward Layered Polymeric Multicomposites. *Science* **1997**, *277*, 1232-1237.

[25] Decher, G.; Multilayer Thin Films: Sequential Assembly of Nanocomposite Materials. In Multilayer Thin Films; Schlenoff, J. Ed.; Wiley-VCH: Weinheim (Germany), 2012.

[26] Xiao, F.-X.; Pagliaro, M.; Xu, Y.-J.; Liu, B. Layer-by-Layer Assembly of Versatile Nanoarchitectures with Diverse Dimensionality: A New Perspective for Rational Construction of Multilayer Assemblies. *Chem. Soc. Rev.* **2016**, *45*, 3088-3121.

[27] Richardson, J. J.; Cui, J.; Björnmalm, M.; Braunger, J. A.; Ejima, H.; Caruso, F. Innovation in Layer-by-Layer Assembly. *Chem. Rev.* **2016**, *116(23)*, 14828-14867.

[28] Lin-Vien D.; Colthup, N.; Fateley, W.; Grasselli, J. The Handbook of Infrared and Roman Characteristic Frequencies of Organic Molecules; Academic press: A Division of Harcourt Brace & Company, San Diego, 1991.

[29] Frey, B. L.; Corn, R. M. Covalent Attachment and Derivatization of Poly(l-lysine) Monolayers on Gold Surfaces As Characterized by Polarization-Modulation FT-IR Spectroscopy. *Anal. Chem*. **1996**, *68(18)*, 3187-3193.

[30.] Xiao, S.; Brunner, S.; Wieland, M. Reactions of Surface Amines with Heterobifunctional Cross-Linkers Bearing Both Succinimidyl Ester and Maleimide for Grafting Biomolecules. *J. Phys. Chem. B* **2004**, *108(42)*, 16508-16517.

[31] Berova, N.; Di Bari, L.; Pescitelli, G. Application of Electronic Circular Dichroism in Configurational and Conformational Analysis of Organic Compounds. *Chem. Soc. Rev.* **2007**, *36(6)*, 914-913.

[32] Arteaga, O.; Ossikovski, R. Complete Mueller Matrix from A Partial Polarimetry Experiment: the 12-Element Case. *J. Opt. Soc. Am. A*, **2019**, *36(3)*, 416-427.

[33] Aas, L. M. S.; Kildemo, M.; Martella, C.; Giordano, M. C.; Chiappe, D.; Buatier de Mongeot, F.; Optical properties of biaxial nanopatterned gold plasmonic nanowired grid polarizer. *Optic Express* **2013**, 21, 30918-30931

[34] Brakstad, T.; Kildemo, M.; Ghadyani, Z.; Simonsen, I.; Dispersion of polarization coupling, localized and collective plasmon modes in a metallic photonic crystal mapped by Mueller Matrix Ellipsometry. *Optics Express* **2015** 23, 22800-22815

[35] Oates, T. W. H.; Ranjan, M.; Facsko, S.; Arwin, H.; Highly anisotropic effective dielectric functions of silver nanoparticle arrays, *Optics Express* **2011**, 19, 2014-2028

[36] Wang, M.; Gompf, B.; Dressel, M.; Destousches, N.; Berrier, A.; Pure circular dichroism by curved rows of plasmonic nanoparticles, *Optical Materials Express* **2018**, 8, 1515-1527

[37] Azzam, R. M. A. Propagation of Partially Polarized Light through Anisotropic Media With or Without Depolarization: A Differential 4 × 4 Matrix Calculus. *J. Opt. Soc. Am.* **1978**, *68(12)*, 1756-1767.

[38] Kuzyk, A.; Schreiber, R.; Fan, Z.; Pardatscher, G.; Roller, E.-M., Högele, A.; Simmel, F. C., Govorov, A. O.; Liedl, T.; DNA-based self-assembly of chiral plasmonic nanostructures with tailored optical response. *Nature* **2012**, 483, 311–314

[39] Schreiber, R.; Luong, N.; Fan, Z.; Kuzyk, A.; Nickels, P. C.; Zhang, T.; Smith, D. M.; Yurke, B.; Kuang, W.; Govorov, A. O.; Liedl, T.; Chiral plasmonic DNA nanostructures with switchable circular dichroism. *Nature Comm.* **2013**, 4, 2948

[40] Buffeteau, T.; Lagugné-Labarthet, F. ; Sourisseau, C. ; Vibrational Circular Dichroism in General Anisotropic Thin Solid Films : Measuremnt and Theoretical Appraoch. *Applied Spectroscopy* **2005**, 59, 732-745

[41] Izquierdo, A.; Ono, S. S.; Voegel, J. C.; Schaaf, P.; Decher, G. Dipping versus Spraying: Exploring the Deposition Conditions for Speeding Up Layer-by-Layer Assembly. *Langmuir* **2005**, *21*, 7558-7567.

[42] Wang, C.; Yan, Q.; Liu, H.-B.; Zhou, X.-H., Xiao, S.-J. Different EDC/NHS Activation Mechanisms between PAA and PMAA Brushes and the Following Amidation Reactions. *Langmuir* **2011**, *27(19)*, 10258-12068.

[43] Broch, L. ; En Naciri, A. ; Johann, L. ; Systematic errors for a Mueller matrix dual rotating compensator ellipsomete. *Opt. Express* **2008**, 16, 8814

[44] Arteaga, O.; Ossikovski, R.; Complete Mueller matrix from a partial polarimetry experiment: the 12-element case. *J. Opt. Soc. Am. A* **2019**, 36, 416

[45] Schneider, C. A.; Rasband, W. S.; Eliceiri, K. W.; NIH Image to ImageJ: 25 years of image analysis. *Nat. Methods* **2012**, 9, 671–675;

[46] Abramoff, M. D.; Magalhaes P. J.; Ram, S. J.. Image processing with ImageJ. *Biophotonics Int.* **2004**, 11, 36–42.

[47] Rezakhaniha, R.; Agianniotis, A. ; Schrauwen, J. T. C. ; Griffa, A. ; Sage, D. ; Bouten, C. V. C. ; Vosse, F. N. ; Unser M. ; Stergiopulos, N. ; Experimental investigation of collagen waviness and orientation in the arterial adventitia using confocal laser scanning microscopy. *Biomech. Model. Mechanobiol.* **2012**, 11, 461–473.